PAPER

CrossMark
click for updates

Homoleptic and heteroleptic *N*-alkylimidazole zinc(II)-containing ionic liquids for high current density electrodeposition†

Marc Steichen,[a] Neil R. Brooks,[b] Luc Van Meervelt,[b] Jan Fransaer[c] and Koen Binnemans*[b]

New homoleptic and heteroleptic zinc(II)-containing liquid metal salts with *N*-alkylimidazole (AlkIm) ligands and bis(trifluoromethylsulfonyl)imide (Tf_2N^-) anions are described. The general formulae of the complexes are $[Zn(AlkIm)_6][Tf_2N]_2$ and $[Zn(AlkIm)_{6-x}(AlkIm')_x][Tf_2N]_2$. Single-crystal X-ray diffraction revealed that, in the solid state, the cations consist of octahedral zinc(II) centres. The heteroleptic complexes contain two different *N*-alkylimidazole ligands. The melting points of the liquid metal salts are below or slightly above room temperature. The dependence of the melting points, viscosity and crystal structure on the alkyl chain length of the *N*-alkylimidazole ligand for the homoleptic complexes and on the ratio of the two *N*-alkylimidazole ligands AlkIm and AlkIm' for the heteroleptic compounds is discussed. The possibility of incongruent melting and the presence of a mixture of the four-coordinate zinc(II) centre and neutral ligands is discussed. The new zinc(II)-containing liquid metal salts have been used as non-aqueous electrolytes for electrodeposition of zinc. A highly reversible deposition–stripping behaviour was found. Zinc electroplating was possible at very high current densities of more than -200 mA cm^{-2} in unstirred solutions. Compact and highly crystalline zinc deposits were obtained.

Introduction

Zinc electroplating (electrogalvanisation) is a widely employed corrosion-protection method for iron and steel parts.[1] Commercial aqueous zinc plating baths allow the electroplating at high current densities. However highly efficient plating baths are typically based on highly toxic cyanide compositions.[1] Less toxic acidic sulphate electrolytes are available, but have lower current efficiencies due to the interfering hydrogen evolution reaction during zinc electrodeposition. In order to fulfil environmental constraints and increase the efficiency of the plating process, alternative plating baths with large metal turn-overs have to be developed.

Ionic liquids (ILs) are salts that are liquid at temperatures below 100 °C.[2,3] They have attracted considerable interest, both in academic and industrial research, as electrolytes for electrodeposition.[4–7] Due to their large electrochemical window, these non-aqueous electrolytes allow the electrodeposition of metals that are impossible (Li, Al, Mg, *etc.*) or difficult (Cr) to electrodeposit from aqueous media due to the interfering hydrogen evolution reaction.[8–10] Moreover, they are characterised by low vapour pressures and high thermal stability allowing the direct electrodeposition at high temperatures without the risk of solvent evaporation.[5,11] Unfortunately many metal salts are poorly soluble in ionic liquids with weakly coordinating anions. One possibility to increase the solubility of metal salts in ionic liquids is by functionalising the cation structure with a coordinating functional group.[12–14] An alternative approach is to incorporate the metal centre directly into the ionic liquid composition. We and others have shown that ionic liquids containing cationic metal complexes are more appropriate for electrochemical applications.[15–19] By incorporation of the metal centre directly into the cationic structure rather than into the anion of an ionic liquid, the metal concentration at the electrochemical interface during the cathodic electrodeposition is increased. We recently reported that copper- and silver-containing ionic liquids with acetonitrile[20,21] and *N*-alkylimidazole[20,22] and alkylamine[19] ligands coordinating to copper(I) and silver(I) centers and the bis(trifluoromethylsulfonyl)imide (Tf_2N^-) anion are excellent electrolytes for high current density electrodeposition.[17,18]

[a]*University of Luxembourg, Laboratory for Energy Materials, 41, rue du Brill, L-4422 Belvaux, Luxembourg*

[b]*KU Leuven, Department of Chemistry, Celestijnenlaan 200F, B-3001 Leuven, Belgium. E-mail: koen.binnemans@chem.kuleuven.be; Fax: +3216327992; Tel: +3216327446*

[c]*KU Leuven, Department of Metallurgy and Materials Engineering, Kasteelpark Arenberg 44, B-3001 Leuven, Belgium*

†Electronic supplementary information (ESI) available: [15]NMR spectra of zinc(II) complexes. CCDC 978387–978391. For ESI and crystallographic data in CIF or other electronic format see DOI: 10.1039/c4dt00182f

In this perspective, the electrodeposition from zinc-based liquid metal salts (Zn-LMS) would be interesting for high speed electrodeposition in added value fabrication processes, such as zinc-containing semiconductor materials. Moreover, highly reversible electroactive zinc-containing electrolytes are of interest for the development of new types of batteries.[23,24] Hsiu *et al.* have shown that the Lewis acidic ionic liquid mixture 1-ethyl-3-methylimidazolium chloride–zinc(II) chloride, $[C_2mim]Cl–ZnCl_2$ with $[ZnCl_2] > 33$ mol%, can be used for the electrodeposition of zinc and zinc-containing alloys at various temperatures.[25] In these Lewis acidic melts, the electroactive zinc(II) species are anionic unsaturated species like $ZnCl_3^-$ and $Zn_2Cl_7^{3-}$. The zinc deposits did not cover the substrate and consisted of hexagonal grains with diameters of 4 to 5 µm. Iwagishi *et al.* studied the electrodeposition of zinc from the Lewis basic ionic liquid mixture $[C_2mim]Br–ZnBr_2$ (70 : 30 mol%) at 120 °C and investigated the effect of added water, ethylene glycol and other dihydric alcohols as diluents.[26,27] Smooth zinc layers were obtained with ethylene glycol and water at cathodic current densities between −10 and −15 mA cm^{-2}. Abbott *et al.* have used the deep-eutectic solvent choline chloride–zinc(II) chloride (1 : 2 molar ratio) to electrodeposit zinc at 60 °C.[28] Due to the high viscosity of the liquid, only low current densities between −2 and −5 mA cm^{-2} were possible and resulted in similar deposit morphologies to those reported by Lin and Sun.[29] In order to improve the bad deposit morphology, Dai *et al.* have recently investigated the influence of different pulse waveforms on the composition and the microstructure of zinc deposits from choline chloride based deep eutectic solvents.[30] Liu *et al.* studied the electrodeposition of zinc films from two ionic liquids namely 1-butyl-1-methylpyrrolidinium trifluoromethylsulfonate $[C_4mpy][TfO]$ and 1-ethyl-3-methylimidazolium trifluoromethylsulfonate $[C_2mim][TfO]$ containing 0.2 M zinc(II) triflate $(Zn(TfO)_2)$ on gold electrodes, as a function of water content and deposition temperature.[31] The authors also used the ionic liquid $[C_4mpy]$-$[TfO]$–0.2 M $Zn(TfO)_2$ to electrodeposit two- and three-dimensional macroporous zinc films in polystyrene templates on gold electrodes.[32]

Only a few examples of cationic low-melting zinc(II) complexes have been reported in the literature so far. Welleman *et al.* have described several four-coordinate *N*-alkylimidazole zinc(II) complexes with different anions (ClO_4^-, BF_4^-, NO_3^-, Br^- and Cl^-), having melting points ranging from 83 to 176 °C,[33] but they have not performed any electrochemical studies. Recently, Pratt *et al.* have described the single-step synthesis of $[Zn(NH_2CH_2CH_2OH)_6][TfO]_2$ in quantitative yield by mixing $Zn(TfO)_2$ and six equivalents of ethanolamine.[16] This zinc(II)-containing ionic liquid had a very high viscosity ($\eta = 2533$ mPa s at 25 °C), so that its electrochemistry could not be studied in an undiluted form but rather as a solution in the ionic liquid $[C_4mim][PF_6]$. Previously, Huang *et al.* reported on the synthesis of the room temperature ionic liquid $[Zn(BuNH_2)_6][Tf_2N]_2$ ($BuNH_2 = n$-butylamine), but no structural information of the Zn(II) complex was given.[34]

In this paper, we describe a series of new zinc(II)-containing homoleptic $[Zn(AlkIm)_6][Tf_2N]_2$ and heteroleptic $[Zn(AlkIm)_{6−x}$-$(AlkIm')_x][Tf_2N]_2$ liquid metal salts (AlkIm and AlkIm' = *N*-alkylimidazole, with MeIm = *N*-methylimidazole, EtIm = *N*-ethylimidazole, BuIm = *N*-butylimidazole; Tf_2N^- = bis-(trifluoromethylsulfonyl)imide), which are suitable as electrolytes for electroplating of zinc at high current densities. In analogy to the traditional dialkylimidazolium ionic liquids, the introduction of two different *N*-alkylimidazoles, differing only in the alkyl chain length, is expected to result in zinc(II) complexes with lower melting points. As shown previously for heteroleptic silver(I)-containing liquid metal salts, the stoichiometry of the obtained complexes relies on the self-assembly of the stoichiometric mixture of the two different *N*-alkylimidazoles used in the synthesis.[20] The change of the melting points, viscosity and crystal structures is discussed as a function of the alkyl chain length of the *N*-alkylimidazole ligand in the homoleptic complexes and as a function of the ratio between the two *N*-alkylimidazole ligands AlkIm and AlkIm' in the heteroleptic compounds. The crystal structures of several zinc(II) complexes are described. The electrochemical properties of the zinc(II)-containing liquids were studied in detail and it is shown that the dense, compact zinc metal layers could be electrodeposited from these liquid metal salts.

Experimental

Zinc oxide, *N*-methylimidazole, and *N*-butylimidazole (ACS reagent grade) were purchased from Sigma-Aldrich (Diegem, Belgium). *N*-Ethylimidazole and hydrogen bis(trifluoromethylsulfonyl)imide (Tf_2NH, 80 wt%) solution in water were obtained from IoLiTec (Heilbronn, Germany). All chemicals were used as received, without further purification. Melting points were determined on Mettler-Toledo 822 DSC apparatus under a helium atmosphere at a heating rate of 10 °C min^{-1}. Elemental analyses (C, H, and N) were performed on a CE Instruments EA-1110 elemental analyser. IR spectra were collected on a Bruker Vertex 70 FTIR spectrometer with a PLATINUM ATR module at a spectral resolution of 4 cm^{-1}. Viscosities were measured on a Brookfield cone plate viscometer (LVDV-II+ programmable viscometer) with a cone spindle CPE-40 under a dry nitrogen atmosphere during measurements with a circulated water bath to control the temperature. Thermogravimetric analysis (TGA) experiments were performed on a TA Q600 instrument and the samples were heated from room temperature to 400 °C at a heating rate of 5 °C min^{-1}. ^1H NMR measurements were performed using a Bruker Avance 300 MHz spectrometer at 25 °C and referenced to tetramethylsilane. ^{15}N NMR spectra were recorded on a Bruker 600 MHz Avance II spectrometer at 60.83 MHz frequency on a BBO 5 mm probe. The pulse program zg was used with a pulse length of 13.7 µs and D1 of 10 seconds. The samples were recorded neat containing a small sealed glass tube of CH_3NO_2 as a standard for the ^{15}N (381.7 ppm) chemical shifts at a temperature of 40 °C for $[Zn(EtIm)_6][Tf_2N]_2$ and

Table 1 Crystal data and structure refinement for the structures of $[Zn(MeIm)_6][Tf_2N]_2$, $[Zn(EtIm)_6][Tf_2N]_2$, $[Zn(MeIm)_1(EtIm)_5][Tf_2N]_2$, $[Zn(MeIm)_2(EtIm)_4][Tf_2N]_2$ and $[Zn(MeIm)_{4.5}(EtIm)_{1.5}][Tf_2N]_2$

	$[Zn(MeIm)_6][Tf_2N]_2$	$[Zn(EtIm)_6][Tf_2N]_2$	$[Zn(MeIm)_1(EtIm)_5]$-$[Tf_2N]_2$	$[Zn(MeIm)_2(EtIm)_4]$-$[Tf_2N]_2$	$[Zn(MeIm)_{4.5}(EtIm)_{1.5}]$-$[Tf_2N]_2$
Empirical formula	$C_{28}H_{36}N_{14}O_8F_{12}S_4Zn$	$C_{34}H_{48}F_{12}N_{14}O_8S_4Zn$	$C_{33}H_{46}N_{14}O_8F_{12}S_4Zn$	$C_{32}H_{44}F_{12}N_{14}O_8S_4Zn$	$C_{29.5}H_{39}F_{12}N_{14}O_8S_4Zn$
Formula weight	1118.32	1202.47	1188.45	1174.42	1139.36
Temperature/K	100(2)	100(2)	100(2)	100(2)	100(2)
Colour	Colourless	Colourless	Colourless	Colourless	Colourless
Size/mm³	0.46 × 0.2 × 0.2	0.35 × 0.35 × 0.25	0.20 × 0.15 × 0.10	0.25 × 0.25 × 0.25	0.62 × 0.05 × 0.05
Crystal system	Monoclinic	Monoclinic	Monoclinic	Monoclinic	Monoclinic
Space group	$P2_1/n$ (no. 14)	$P2_1/c$ (no. 14)	$P2_1/c$ (no. 14)	$P2_1/c$ (no. 14)	$P2_1/c$ (no. 14)
a/Å	8.1827(1)	11.0834(5)	11.0036(3)	10.9682(4)	8.3667(2)
b/Å	20.1947(3)	11.1196(4)	11.1127(3)	11.1202(4)	11.5721(3)
c/Å	27.0549(3)	20.2237(7)	20.1049(5)	20.0576(6)	24.0909(4)
α/°	90	90	90	90	90
β/°	92.441(1)	98.423(4)	98.316(2)	98.463(3)	95.811(2)
γ/°	90	90	90	90	90
Volume/Å³	4466.69(9)	2465.56(17)	2432.58(11)	2419.76(13)	2320.49(9)
Z	4	2	2	2	2
ρ_{calc} Mg/m³	1.663	1.620	1.623	1.612	1.631
μ/mm⁻¹	0.849	0.776	0.785	0.788	0.819
Wavelength	0.71073	0.71073	0.71073	0.71073	0.71073
Reflections collected	22 708	11 408	11 191	19 840	10 876
Independent reflections	10 303	5605	5586	5822	5326
R(int)	0.0189	0.0197	0.0142	0.0177	0.0161
R_1 [$I \geq 2\sigma(I)$]	0.0293	0.0273	0.0268	0.0256	0.0511
wR_2 [all data]	0.0701	0.0675	0.0678	0.0647	0.1383
Goof	1.054	1.033	1.050	1.030	1.035
$\Delta\rho_{max,min}$/e Å⁻³	0.45/−0.34	0.36/−0.38	0.45/−0.42	0.40/−0.46	0.89/−0.74

$[Zn(BuIm)_6][Tf_2N]_2$, and 70 °C for $[Zn(MeIm)_6][Tf_2N]_2$. Electrochemical experiments were performed in an argon-filled glove box with oxygen and water levels below 1 ppm. A platinum-covered silicon wafer was used as a working electrode. Zinc wires served as counter and reference electrodes (pseudo-reference). The temperature-controlled (90 °C) three-electrode setup was connected to an Ecochemie Autolab PGSTAT302N potentiostat, equipped with the GPES software for cyclic voltammetry and chronopotentiometry measurements. For electrodeposition, the platinum electrode was inserted in a poly-(tetrafluoroethylene) (PTFE) holder with a recess channel in order to decrease the tendency of dendrite formation, by creating a uniform primary current density distribution over the electrode surface. A picture of the setup can be found in ref. 17. X-ray diffraction (XRD) measurements of the deposits were performed on a Bruker Discover D8 Diffractometer with a Cu K$_{\alpha 1/2}$ source ($\lambda_{\alpha 1}$ = 1.54056 Å) and a scintillation detector in the θ–2θ configuration. Scanning Electron Microscopy (SEM) was performed on Hitachi SU-70 apparatus equipped with an Oxford Instruments INCA X-MAX analyser for Energy-Dispersive X-ray spectroscopy (EDX).

Crystals of complexes $[Zn(MeIm)_6][Tf_2N]_2$, $[Zn(EtIm)_6]$-$[Tf_2N]_2$, $[Zn(MeIm)(EtIm)_5][Tf_2N]_2$, $[Zn(MeIm)_2(EtIm)_4][Tf_2N]_2$ and $[Zn(MeIm)_{4.5}(EtIm)_{1.5}][Tf_2N]_2$ suitable for single crystal X-ray diffraction were mounted on a nylon loop attached to a copper pin and placed into the cold stream of an Oxford Cryostream 700 at 100(2) K on an Agilent SuperNova diffractometer using Mo Kα radiation (λ = 0.71073 Å). The absorption corrections were applied using CrysAlisPro.[35] All structures were solved using direct methods and refined by the full-matrix least-squares procedure in SHELXL.[36] All hydrogen atoms were placed in calculated positions and refined using a riding model. Description of the disorder modelling for the hetero-leptic compounds is given in the main text. A summary of the crystallographic data can be found in Table 1. CCDC 978387–978391 contains the supplementary crystallographic data for this paper. The program OLEX2 was also used in refinement and making pictures.[37]

Synthesis of $[Zn(H_2O)_6][Tf_2N]_2 \cdot 2H_2O$

An 80 wt% HTf$_2$N (24.0 g, 85.4 mmol) solution was added to a suspension of zinc(II) oxide (6.08 g, 74.6 mmol) in water (80 mL). The solution was heated for 16 hours at 80 °C. The excess of zinc(II) oxide was filtered off after reaction. Then, the solvent was removed *in vacuo* and after cooling the product precipitated and was dried *in vacuo* at room temperature. Yield: 29.91 g (38.86 mmol, 91%); Elemental analysis: ($C_4H_{16}F_{12}N_2O_{16}S_4Zn$) calculated: C: 6.24%, H: 2.09%, N: 3.64%; found: C: 6.64%, H: 2.11%, N: 3.61%; IR (ATR/cm⁻¹): 3483, 1633, 1336, 1193, 1123, 1039, 795, 770, 744, 653, 612, 570, 507.

Synthesis of $[Zn(MeIm)_6][Tf_2N]_2$

$[Zn(H_2O)_6][Tf_2N]_2 \cdot 2H_2O$ (1.48 g, 1.92 mmol) and 1-methylimidazole (0.948 g, 11.54 mmol) were mixed together in ethanol (20 mL) for 1 hour at room temperature. The solvent was removed *in vacuo* to give $[Zn(MeIm)_6][Tf_2N]_2$ (2.13 g, 1.90 mmol; 99%). Melting point: 65 °C; Elemental analysis:

($C_{28}H_{36}F_{12}N_{14}O_8S_4Zn$) calculated: C: 30.05%, H: 3.24%, N: 17.53%; found: C: 29.47%, H: 2.92%, N: 17.05%; ^{1}H NMR δ/ppm (300 MHz, CD_3OD): 7.96 (s, 6H), 7.33 (s, 6H), 7.10 (s, 6H), 3.83 (s, 18H); ^{15}N NMR δ/ppm (60.83 MHz): 215.8, 167.0, 140.6; IR (ATR/cm^{-1}): 3139, 1590, 1548, 1530, 1475, 1426, 1348, 1330, 1292, 1227, 1177, 1134, 1098, 1052, 958, 935, 833, 789, 740, 671, 655, 611, 599, 569, 509, 407. Crystals suitable for X-ray diffraction were grown from the melt.

Synthesis of [Zn(EtIm)$_6$][Tf$_2$N]$_2$

[Zn(H$_2$O)$_6$][Tf$_2$N]$_2$·2H$_2$O (1.44 g, 1.87 mmol) and 1-ethylimidazole (1.08 g, 11.25 mmol) were mixed together in ethanol (20 mL) for 1 hour at room temperature. The solvent was removed *in vacuo* to give [Zn(EtIm)$_6$][Tf$_2$N]$_2$ (2.23 g, 1.85 mmol; 99%). Melting point: 35 °C; Elemental analysis: ($C_{34}H_{48}F_{12}N_{14}O_8S_4Zn$) calculated: C: 33.96%, H: 4.02%, N: 16.30%; found: C: 33.51%, H: 2.71%, N: 15.76%; ^{1}H NMR δ/ppm (300 MHz, CD_3OD): 8.05 (s, 6H), 7.38 (s, 6H), 7.11 (s, 6H), 4.17 (q, 12H, ^3J = 7.3 Hz), 1.46 (t, 18H, ^3J = 7.3 Hz); ^{15}N NMR δ/ppm (60.83 MHz): 215.1, 183.5, 139.8; IR (ATR/cm^{-1}): 3136, 2987, 1600, 1539, 1527, 1468, 1450, 1389, 1348, 1331, 1228, 1179, 1135, 1110, 1097, 1053, 963, 935, 909, 832, 788, 740, 653, 613, 600, 569, 510, 406. Crystals suitable for X-ray diffraction were grown from the melt.

Synthesis of [Zn(MeIm)$_5$(EtIm)$_1$][Tf$_2$N]$_2$

[Zn(H$_2$O)$_6$][Tf$_2$N]$_2$·2H$_2$O (1.18 g, 1.53 mmol), 1-methylimidazole (0.629 g, 7.66 mmol) and 1-ethylimidazole (0.147 g, 1.53 mmol) were mixed together in ethanol (20 mL) for 1 hour at room temperature. The solvent was removed *in vacuo* to give [Zn(MeIm)$_5$(EtIm)$_1$][Tf$_2$N]$_2$ (1.70 g, 1.50 mmol; 98%). Melting point: 64 °C; Elemental analysis: ($C_{29}H_{38}F_{12}N_{14}O_8S_4Zn$) calculated: C: 30.76%, H: 3.38%, N: 17.32%; found: C: 30.08%, H: 3.29%, N: 16.65%; ^{1}H NMR δ/ppm (300 MHz, CD_3OD): 8.06 (s, 1H), 7.99 (s, 5H), 7.43 (s, 1H), 7.35 (s, 5H), 7.12 (s, 1H), 7.11 (s, 5H), 4.19 (q, 2H, ^3J = 7.3 Hz), 3.84 (s, 15H), 1.49 (t, 3H, ^3J = 7.3 Hz); IR (ATR/cm^{-1}): 3138, 2965, 1597, 1531, 1518, 1468, 1426, 1349, 1332, 1287, 1227, 1173, 1139, 1108, 1088, 1052, 959, 935, 830, 790, 744, 661, 655, 609, 569, 513, 409.

Synthesis of [Zn(MeIm)$_4$(EtIm)$_2$][Tf$_2$N]$_2$

[Zn(H$_2$O)$_6$][Tf$_2$N]$_2$·2H$_2$O (1.19 g, 1.55 mmol), 1-methylimidazole (0.509 g, 6.19 mmol) and 1-ethylimidazole (0.298 g, 3.09 mmol) were mixed together in ethanol (20 mL) for 1 hour at room temperature. The solvent was removed *in vacuo* to give [Zn(MeIm)$_4$(EtIm)$_2$][Tf$_2$N]$_2$ (1.75 g, 1.54 mmol; 99%). Melting point: 49 °C; Elemental analysis: ($C_{30}H_{40}F_{12}N_{14}O_8S_4Zn$) calculated: C: 31.43%, H: 3.52%, N: 17.10%; found: C: 31.13%, H: 3.28%, N: 16.69%; ^{1}H NMR δ/ppm (300 MHz, CD_3OD): 8.06 (s, 2H), 7.99 (s, 4H), 7.43 (s, 2H), 7.34 (s, 4H), 7.12 (s, 2H), 7.11 (s, 4H), 4.19 (q, 4H, ^3J = 7.3 Hz), 3.84 (s, 12H), 1.49 (t, 6H, ^3J = 7.3 Hz); IR (ATR/cm^{-1}): 3137, 2966, 1597, 1531, 1518, 1469, 1426, 1349, 1332, 1287, 1227, 1173, 1139, 1108, 1087, 1052, 959, 935, 830, 790, 743, 661, 610, 569, 513, 408. Some crystals of [Zn(MeIm)$_{4.5}$(EtIm)$_{1.5}$][Tf$_2$N]$_2$ suitable for X-ray diffraction were grown from the melt.

Synthesis of [Zn(MeIm)$_3$(EtIm)$_3$][Tf$_2$N]$_2$

[Zn(H$_2$O)$_6$][Tf$_2$N]$_2$·2H$_2$O (1.79 g, 2.32 mmol), 1-methylimidazole (0.572 g, 6.97 mmol) and 1-ethylimidazole (0.670 g, 6.97 mmol) were mixed together in ethanol (20 mL) for 1 hour at room temperature. The solvent was removed *in vacuo* to give [Zn(MeIm)$_3$(EtIm)$_3$][Tf$_2$N]$_2$ (2.69 g, 2.31 mmol; 99%). Melting point: 35 °C; Elemental analysis: ($C_{31}H_{42}F_{12}N_{14}O_8S_4Zn$) calculated: C: 32.09%, H: 3.65%, N: 16.90%; found: C: 31.68%, H: 3.71%, N: 16.31%; ^{1}H NMR δ/ppm (300 MHz, CD_3OD): 8.00 (s, 3H), 7.93 (s, 3H), 7.38 (s, 3H), 7.30 (s, 3H), 7.08 (s, 3H), 7.07 (s, 3H), 4.15 (q, 6H, ^3J = 7.3 Hz), 3.81 (s, 9H), 1.46 (t, 9H, ^3J = 7.3 Hz); IR (ATR/cm^{-1}): 3136, 2968, 1597, 1531, 1517, 1469, 1427, 1348, 1332, 1287, 1227, 1173, 1139, 1108, 1088, 1052, 960, 935, 830, 790, 742, 661, 655, 609, 569, 512, 409. Some crystals of [Zn(MeIm)$_{4.5}$(EtIm)$_{1.5}$][Tf$_2$N]$_2$ suitable for X-ray diffraction were grown from the melt.

Synthesis of [Zn(MeIm)$_2$(EtIm)$_4$][Tf$_2$N]$_2$

[Zn(H$_2$O)$_6$][Tf$_2$N]$_2$·2H$_2$O (2.12 g, 2.75 mmol), 1-methylimidazole (0.452 g, 5.50 mmol) and 1-ethylimidazole (1.06 g, 11.00 mmol) were mixed together in ethanol (20 mL) for 1 hour at room temperature. The solvent was removed *in vacuo* to give [Zn(MeIm)$_2$(EtIm)$_4$][Tf$_2$N]$_2$ (3.20 g, 2.73 mmol; 99%). Melting point: 20 °C; Elemental analysis: ($C_{32}H_{44}F_{12}N_{14}O_8S_4Zn$) calculated: C: 32.73%, H: 3.78%, N: 16.70%; found: C: 32.57%, H: 3.46%, N: 16.68%; ^{1}H NMR δ/ppm (300 MHz, CD_3OD): 8.08 (s, 4H), 8.01 (s, 2H), 7.44 (s, 4H), 7.35 (s, 2H), 7.13 (s, 4H), 7.12 (s, 3H), 4.20 (q, 8H, ^3J = 7.3 Hz), 3.85 (s, 6H), 1.49 (t, 12H, ^3J = 7.3 Hz); IR (ATR/cm^{-1}): 3137, 2988, 1685, 1620, 1523, 1469, 1451, 1422, 1405, 1345, 1323, 1289, 1232, 1174, 1134, 1104, 1092, 1059, 1034, 961, 933, 836, 788, 764, 742, 663, 651, 619, 597, 570, 506, 439, 409. Crystals suitable for X-ray diffraction were grown from the melt in a refrigerator at 4 °C over the period of several days.

Synthesis of [Zn(MeIm)$_1$(EtIm)$_5$][Tf$_2$N]$_2$

[Zn(H$_2$O)$_6$][Tf$_2$N]$_2$·2H$_2$O (1.78 g, 2.31 mmol), 1-methylimidazole (0.189 g, 2.31 mmol) and 1-ethylimidazole (1.11 g, 11.54 mmol) were mixed together in ethanol (20 mL) for 1 hour at room temperature. The solvent was removed *in vacuo* to give [Zn(MeIm)$_1$(EtIm)$_5$][Tf$_2$N]$_2$ (2.72 g, 2.29 mmol; 99%). Melting point: 29 °C; Elemental analysis: ($C_{33}H_{46}F_{12}N_{14}O_8S_4Zn$) calculated: C: 33.35%, H: 3.90%, N: 16.50%; found: C: 32.87%, H: 3.54%, N: 16.24%; ^{1}H NMR δ/ppm (300 MHz, CD_3OD): 8.09 (s, 5H), 8.02 (s, 1H), 7.44 (s, 5H), 7.35 (s, 1H), 7.14 (s, 5H), 7.13 (s, 1H), 4.21 (q, 10H, ^3J = 7.3 Hz), 3.85 (s, 3H), 1.49 (t, 15H, ^3J = 7.3 Hz); IR (ATR/cm^{-1}): 3137, 2987, 1684, 1618, 1524, 1469, 1454, 1405, 1345, 1323, 1289, 1231, 1175, 1133, 1112, 1094, 1058, 1034, 962, 933, 837, 788, 762, 740, 663, 652, 618, 598, 570, 506, 441, 404. Crystals suitable for X-ray diffraction were grown from the melt in a refrigerator.

Synthesis of [Zn(BuIm)$_6$][Tf$_2$N]$_2$

[Zn(H$_2$O)$_6$][Tf$_2$N]$_2$·2H$_2$O (1.02 g, 1.33 mmol) and 1-butylimidazole (0.988 g, 7.96 mmol) were mixed together in ethanol

(20 mL) for 1 hour at room temperature. The solvent was removed *in vacuo* to give $[Zn(BuIm)_6][Tf_2N]_2$ (1.78 g, 1.30 mmol; 98%). Melting point: <RT; Elemental analysis: $(C_{46}H_{72}F_{12}N_{14}O_8S_4Zn)$ calculated: C: 40.30%, H: 5.29%, N: 14.30%; found: C: 39.47%, H: 4.77%, N: 14.08%; ^1H NMR δ/ppm (300 MHz, CD_3OD): 7.89 (s, 6H), 7.12 (s, 6H), 7.03 (s, 6H), 4.06 (t, 12H, ^3J = 7.3 Hz), 1.80 (quin, 12H, ^3J = 7.3 Hz), 1.34 (sex, 12H, ^3J = 7.3 Hz), 0.93 (t, 18H, ^3J = 7.3 Hz); ^{15}N NMR δ/ppm (60.83 MHz): 204.0, 182.7, 139.9; IR (ATR/cm^{-1}): 3134, 2963, 2937, 2877, 1597, 1526, 1462, 1349, 1331, 1227, 1180, 1136, 1096, 1054, 957, 936, 909, 831, 788, 739, 656, 614, 600, 569, 510, 406.

Results and discussion

General methods for the synthesis of the zinc(II) complexes

The hydrated zinc(II) bis(trifluoromethylsulfonyl)imide salt $[Zn(H_2O)_6][Tf_2N]_2 \cdot 2H_2O$ was dissolved in a minimum volume of ethanol and an appropriate amount (1 : 6 metal to ligand stoichiometry) of N-alkylimidazole ligand was added. The complexation reaction was allowed to proceed for one hour at room temperature and afterwards the solution was concentrated on a rotary evaporator and where possible a solid was collected and dried *in vacuo* for two days. For compounds with melting points close to room temperature, a liquid was collected and was further dried *in vacuo* for two days. If no solidification occurred, the liquid was placed in a fridge for a few days. All complexes studied in this work have a 1 : 6 metal-to-ligand ratio, even though zinc(II) metal centers can be six-, five- and four-coordinate. It has been shown that four-coordinate zinc(II) complexes are extremely viscous and decompose rapidly in air, so they were not investigated by us.[16]

Crystal structures

Single crystals of the homoleptic complexes $[Zn(MeIm)_6][Tf_2N]_2$ and $[Zn(EtIm)_6][Tf_2N]_2$ could be grown from the respective melts. The structure of $[Zn(MeIm)_6][Tf_2N]_2$ was found to consist of octahedral cationic metal centres with two Tf_2N^- anions and is isostructural to the previously reported $[M(MeIm)_6][Tf_2N]_2$ (M = Co, Ni).[22] Although isostructural, the nickel(II) analogue was reported to be found exclusively as a non-merohedrally twinned crystals, whereas the crystals of the cobalt(II) analogue did not show twinning. Crystals of $[Zn(MeIm)_6][Tf_2N]_2$ were not twinned either. The M–N bond distances were found to be similar to the previously reported Co and Ni structures (Zn–N = 2.1588(13)–2.1973(13) Å; Co–N = 2.1467(14)–2.1779(13) Å; Ni–N = 2.104(3)–2.138(3) Å).[22] The structure of $[Zn(EtIm)_6][Tf_2N]_2$ was found to have the same octahedral coordination (Fig. 1) as $[Zn(MeIm)_6][Tf_2N]_2$, except that the zinc(II) centre of $[Zn(EtIm)_6][Tf_2N]_2$ lies on a crystallographic inversion centre, meaning that the asymmetric unit consists of one half cation and one Tf_2N^- anion. The Zn–N distances are 2.1657(12)–2.1995(12) Å, which are very similar to those of $[Zn(MeIm)_6][Tf_2N]_2$.
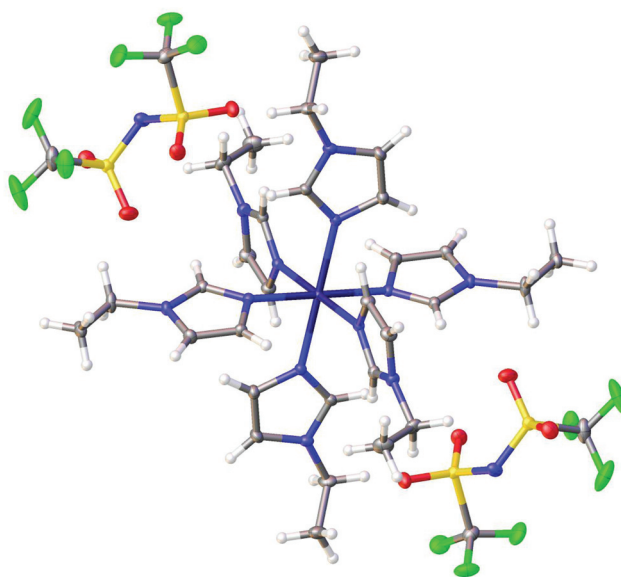

Fig. 1 View of the crystal structure of $[Zn(EtIm)_6][Tf_2N]_2$ showing a cation and two anions. Displacement ellipsoids are shown at the 50% probability level (zinc royal blue, nitrogen blue, sulphur yellow, oxygen red, fluorine green, carbon grey and hydrogen white).

The crystal structures of the heteroleptic compounds were found to be more complicated. This is mostly due to the positional disorder of the MeIm and EtIm ligands. This type of disorder was found in the crystal structures of the heteroleptic silver(I) compounds $[Ag(MeIm)(BuIm)][Tf_2N]$ and $[Ag(EtIm)(BuIm)][Tf_2N]$,[20] but in that case, with the silver(I) compounds being only two-coordinate, modelling of the disorder in the crystal structure refinements was much easier. Another possibility is that ligand exchange can occur in the liquid state and there is an equilibrium between different species. For example two molecules of the compound $[Zn(MeIm)_2(EtIm)_4][Tf_2N]_2$ could form a molecule of $[Zn(MeIm)_1(EtIm)_5][Tf_2N]_2$ and $[Zn(MeIm)_3(EtIm)_3][Tf_2N]_2$. This mixture of compounds could be preserved in the solid state so that the crystal structure comprises a mixture of compounds. This ligand exchange process may also give rise to preferential crystallisation of compounds with a different ligand ratio from the bulk. This was also observed in the case of the silver(I) liquid metal salts of the composition $[Ag(py-O)_3][X]$ (py-O = pyridine-N-oxide; X = NO_3, CH_3SO_3, CF_3SO_3).[38]

Single crystals of the heteroleptic complexes $[Zn(MeIm)_1(EtIm)_5][Tf_2N]_2$, $[Zn(MeIm)_2(EtIm)_4][Tf_2N]_2$ and $[Zn(MeIm)_{4.5}(EtIm)_{1.5}][Tf_2N]_2$ could be grown and studied. In the cases of $[Zn(MeIm)_1(EtIm)_5][Tf_2N]_2$ and $[Zn(MeIm)_2(EtIm)_4][Tf_2N]_2$ the crystals came from liquids of the same composition, but in the case of $[Zn(MeIm)_{4.5}(EtIm)_{1.5}][Tf_2N]_2$ these crystals were found in samples where the composition of the liquid was both $[Zn(MeIm)_3(EtIm)_3][Tf_2N]_2$ and $[Zn(MeIm)_4(EtIm)_2][Tf_2N]_2$.

The crystal structures of $[Zn(MeIm)_1(EtIm)_5][Tf_2N]_2$ and $[Zn(MeIm)_2(EtIm)_4][Tf_2N]_2$ both crystallised in a similar monoclinic crystal system, which was also similar to that of $[Zn(EtIm)_6][Tf_2N]_2$ (Table 1). There were important differences in

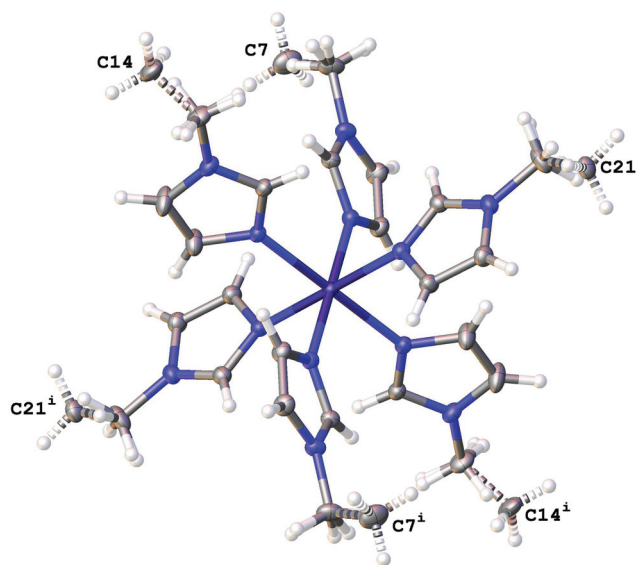the crystal structures of the heteroleptic compounds compared to the structure of $[Zn(EtIm)_6][Tf_2N]_2$, which showed that it was not simply $[Zn(EtIm)_6][Tf_2N]_2$ that had crystallised from the heteroleptic liquids. Firstly, looking at the total volumes of the crystal unit cells (Table 1), it can be clearly seen that there is a large decrease in the unit cell volume between $[Zn(EtIm)_6]$-$[Tf_2N]_2$ ($V = 2465.56(17)$ Å^3), $[Zn(MeIm)_1(EtIm)_5][Tf_2N]_2$ ($V = 2432.58(11)$ Å^3) and $[Zn(MeIm)_2(EtIm)_4][Tf_2N]_2$ ($V = 2419.76(13)$ Å^3). Although the first difference of 16.5 Å^3 per methylene unit is close to the expected 18 Å^3, the second smaller change of 6.5 Å^3 is still significant. Secondly, if the heteroleptic structures were simply refined as $[Zn(EtIm)_6][Tf_2N]_2$ then the thermal parameters for the terminal CH$_3$ groups on the ethyl chains became very large, indicating that there is less electron density present than is trying to be modelled. The site occupancies of the terminal CH$_3$ of the ethyl groups were investigated further to determine the coordination position of the MeIm/EtIm ligands or the extent of MeIm/EtIm disorder at each position. To understand this further, the crystallographic symmetry of the cation must be considered because the cations sit on crystallographic inversion centres. The crystallographic asymmetric unit consists of one half cation and the other half is generated by the crystallographic symmetry (Fig. 2). At each of these three coordination sites (and their symmetry equivalents) there could be either a MeIm or a EtIm ligand (Fig. 2). To determine the amount of EtIm in each position, the occupancy of the CH$_3$ groups at the positions C7, C14 and C21 (Fig. 2) was allowed to freely refine. The sum of the occupancies of the carbon atoms at these three positions gives the total amount of EtIm in the crystal. It was found that the EtIm had a preference for the C7 position, where there was

Fig. 2 View of the disorder as seen in the cation of the crystal structures of $[Zn(MeIm)_1(EtIm)_5][Tf_2N]_2$ and $[Zn(MeIm)_2(EtIm)_4][Tf_2N]_2$ (symmetry code: i 1 − x, −y, −z). Displacement ellipsoids are shown at the 50% probability level (zinc royal blue, nitrogen blue, carbon grey and hydrogen white).

Table 2 Unrestrained refinement of the occupancies of the EtIm CH$_3$ groups in the structures of $[Zn(MeIm)_1(EtIm)_5][Tf_2N]_2$ and $[Zn(MeIm)_2(EtIm)_4][Tf_2N]_2$. The restrained values of $[Zn(EtIm)_6][Tf_2N]_2$ are given for comparison

	$[Zn(EtIm)_6]$-$[Tf_2N]_2$	$[Zn(MeIm)_1(EtIm)_5]$-$[Tf_2N]_2$	$[Zn(MeIm)_2(EtIm)_4]$-$[Tf_2N]_2$
C7	1	0.981(7)	0.946(7)
C14	1	0.855(7)	0.674(6)
C21	1	0.708(6)	0.435(6)
Total	3	2.544	2.055

very little amount of MeIm (occupancies: 0.981 ($[Zn(MeIm)_1$-$(EtIm)_5][Tf_2N]_2$) and 0.946 ($[Zn(MeIm)_2(EtIm)_4][Tf_2N]_2$); Table 2). The other two positions C14 and C21 showed some degree of disorder between MeIm and EtIm (Table 2). The sum of the refined occupancies gives the overall MeIm/EtIm content of the crystal and shows that the crystals contain approximately the same composition of EtIm and MeIm as the liquids from which they were grown (Table 2). For the final refinement of the crystal structures, the MeIm : EtIm ratio was fixed to be the same as the composition of the liquids. Although the composition of the crystal structures has been determined to be $[Zn(MeIm)_1(EtIm)_5][Tf_2N]_2$ and $[Zn(MeIm)_2$-$(EtIm)_4][Tf_2N]_2$, it is certainly possible that the structures also contain an amount of other Zn(II) complexes. For example $[Zn(MeIm)_1(EtIm)_5][Tf_2N]_2$ could contain an amount of $[Zn(EtIm)_6][Tf_2N]_2$ and $[Zn(MeIm)_2(EtIm)_4][Tf_2N]_2$. The fact that the heteroleptic structures are isostructural to $[Zn(EtIm)_6]$-$[Tf_2N]_2$ suggests that the structure is flexible enough to allow, to a certain extent, substitution of EtIm for MeIm ligands. Evidence for this can be seen by looking at the crystal packing. The packing motif is that the cations make sheets in the *bc* plane with the Tf$_2$N$^-$ anions occupying positions between these sheets (Fig. 3). It can be seen that the positions of the EtIm groups containing C7 (shown with normal bonds and no disorder in Fig. 3) are within these sheets. The EtIm groups containing C14 (dashed lines in Fig. 3) and C21 (thin solid lines in Fig. 3) point out from the sheet towards the Tf$_2$N$^-$ anions allowing partial contraction of the structure.

From the crystal structures of $[Zn(MeIm)_1(EtIm)_5][Tf_2N]_2$ and $[Zn(MeIm)_2(EtIm)_4][Tf_2N]_2$, there was a good correlation between the composition obtained from the structure refinement and the composition of the liquid. However, this was not the case for crystals grown from liquids with other MeIm : EtIm ratios. For the liquids of compositions $[Zn(MeIm)_3$-$(EtIm)_3][Tf_2N]_2$ and $[Zn(MeIm)_4(EtIm)_2][Tf_2N]_2$, crystals with an approximate composition $[Zn(MeIm)_{4.5}(EtIm)_{1.5}][Tf_2N]_2$ were obtained. The crystal structure of $[Zn(MeIm)_{4.5}(EtIm)_{1.5}][Tf_2N]_2$ has a completely different unit cell, and hence a different structure, from that of $[Zn(MeIm)_6][Tf_2N]_2$, $[Zn(EtIm)_6][Tf_2N]_2$ or the heteroleptic compounds just described (Table 1). In $[Zn$-$(MeIm)_{4.5}(EtIm)_{1.5}][Tf_2N]_2$, the cation sits on a crystallographic inversion so there is only half of the cation in the asymmetric unit. Like in the other heteroleptic compounds, if the structure is refined as containing all MeIm ligands then residual
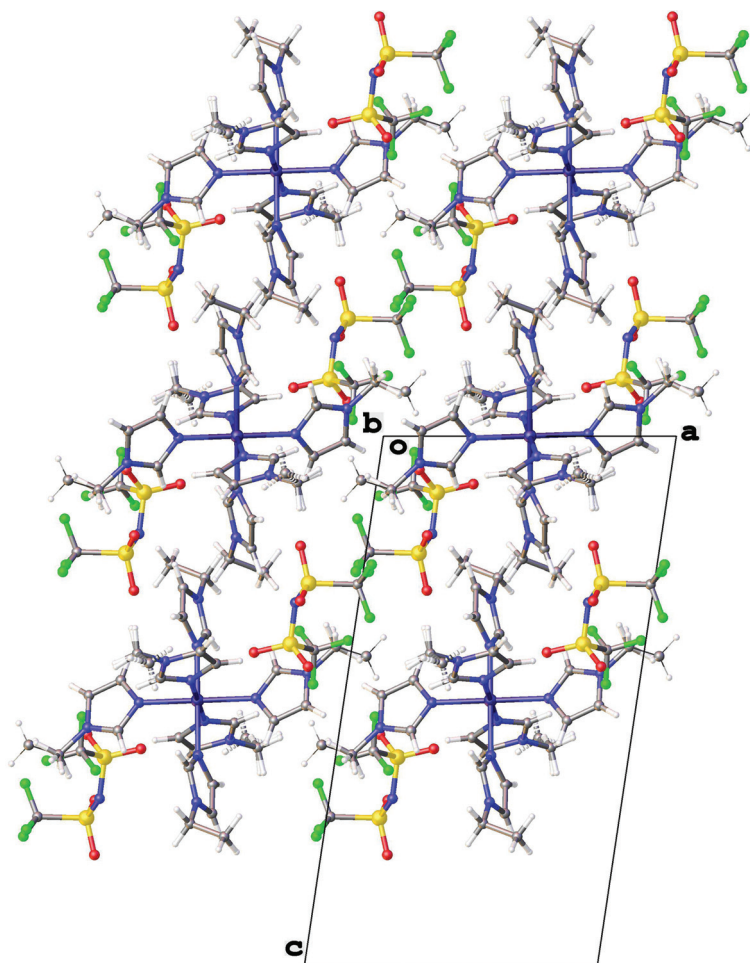
Fig. 3 View of the packing in the crystal structure of $[Zn(MeIm)_2(EtIm)_4]$-$[Tf_2N]_2$ (disorder of the C7 position not shown, bonds to C14 shown as dashed lines, bonds to C21 shown as thin solid lines; zinc royal blue, nitrogen blue, sulphur yellow, oxygen red, fluorine green, carbon grey and hydrogen white).

difference electron density peaks occur where the CH_3 groups of EtIm would be expected, and if refined as all EtIm then the terminal CH_3 groups have high thermal displacement parameters. Applying a similar refinement strategy to that described for the previous heteroleptic compounds, the occupancies of the CH_3 group of EtIm in the three possible coordination positions refine to one position being approximately half occupied and the other two are just over 10% occupied (Table 3). Due to the low occupancy in two positions, restraints were required in the refinement to keep sensible C–C bond distances and thermal parameters. The sum of the refined

occupancies indicated that the MeIm : EtIm ratio was approximately 4.5 : 1.5 and this ratio was fixed in the final refinement to give rounded number of ligands. Several crystals of this type could be found from the liquids of compositions $[Zn(MeIm)_3$-$(EtIm)_3][Tf_2N]_2$ and $[Zn(MeIm)_4(EtIm)_2][Tf_2N]_2$, and in all cases the refined occupancies of the crystal data gave a formula of approximately $[Zn(MeIm)_{4.5}(EtIm)_{1.5}][Tf_2N]_2$. Single crystals of other compositions could not be found crystallising in the liquids of compositions $[Zn(MeIm)_3(EtIm)_3][Tf_2N]_2$ and $[Zn$-$(MeIm)_4(EtIm)_2][Tf_2N]_2$. The compound of an overall formula $[Zn(MeIm)_{4.5}(EtIm)_{1.5}][Tf_2N]_2$ cannot contain a Zn(II) centre with 1.5 ligands coordinated so this structure must contain a mixture of compounds and is most likely to predominantly be a 50 : 50 mixture of $[Zn(MeIm)_4(EtIm)_2][Tf_2N]_2$ and $[Zn(MeIm)_5$-$(EtIm)_1][Tf_2N]_2$.

Looking at the packing of $[Zn(MeIm)_{4.5}(EtIm)_{1.5}][Tf_2N]_2$, there is a similar pattern to that seen before (Fig. 4). The packing motif shows sheets of cations (in the *ab* plane) with Tf_2N^- anions in between. The position of C7 is such that it lies with the plane of the cations and the positions of C14 and C21 point towards the Tf_2N^- anions.

Table 3 Unrestrained refinement of the occupancies of the EtIm CH_3 groups in the structure of $[Zn(MeIm)_{4.5}(EtIm)_{1.5}][Tf_2N]_2$ when the crystals were grown from $[Zn(MeIm)_3(EtIm)_3][Tf_2N]_2$ or $[Zn(MeIm)_4(EtIm)_2][Tf_2N]_2$

	$[Zn(MeIm)_3(EtIm)_3][Tf_2N]_2$	$[Zn(MeIm)_4(EtIm)_2][Tf_2N]_2$
C7	0.52(2)	0.52(2)
C14	0.112(11)	0.113(11)
C21	0.112(14)	0.114(15)
Total	0.744	0.747
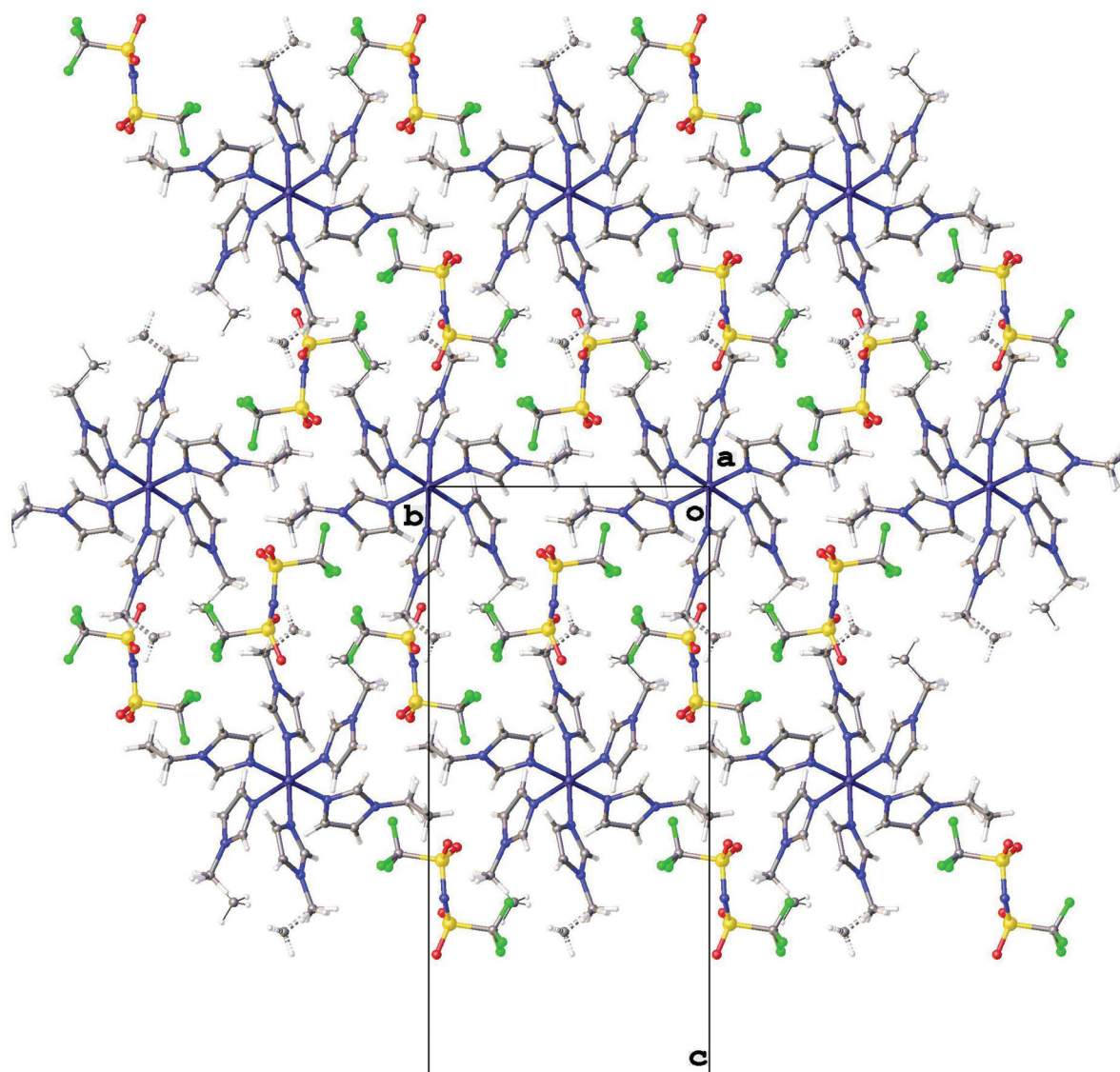
Fig. 4 View of the packing in the crystal structure of [Zn(MeIm)$_{4.5}$(EtIm)$_{1.5}$][Tf$_2$N]$_2$ (bonds to C7 shown as normal lines, bonds to C14 shown as dashed lines, bonds to C21 shown as thin solid lines; zinc royal blue, nitrogen blue, sulphur yellow, oxygen red, fluorine green, carbon grey and hydrogen white).

Thermal properties and viscosities

The trend for the melting points of the homoleptic [Zn-(AlkIm)$_6$][Tf$_2$N]$_2$ compounds is that the melting point decreases as the alkyl chain length increases from 65 °C for [Zn(MeIm)$_6$][Tf$_2$N]$_2$ to 35 °C for [Zn(EtIm)$_6$][Tf$_2$N]$_2$ to below room temperature for [Zn(BuIm)$_6$][Tf$_2$N]$_2$. No evidence of solidification for [Zn(BuIm)$_6$][Tf$_2$N]$_2$ was found, even on cooling to −60 °C. For sufficiently long alkyl chain length, the melting points are expected to increase again, in analogy to imidazolium-based ionic liquids.[2] A compound with a lower melting temperature than [Zn(MeIm)$_6$][Tf$_2$N]$_2$ can be synthesised by replacing one or more of the MeIm ligands by an N-alkylimidazole with a longer chain. Table 4 shows how the melting point varies with the constituency of the complex for the series of heteroleptic compounds [Zn(MeIm)$_{6-x}$(EtIm)$_x$]-[Tf$_2$N]$_2$. The [Zn(MeIm)$_2$(EtIm)$_4$][Tf$_2$N]$_2$ compound has a

Table 4 Melting points of the homoleptic [Zn(AlkIm)$_6$][Tf$_2$N]$_2$ and heteroleptic [Zn(MeIm)$_{6-x}$(AlkIm)$_x$][Tf$_2$N]$_2$ complexes

Compound	T_m (°C)
[Zn(MeIm)$_6$][Tf$_2$N]$_2$	65
[Zn(MeIm)$_5$(EtIm)$_1$][Tf$_2$N]$_2$	64
[Zn(MeIm)$_4$(EtIm)$_2$][Tf$_2$N]$_2$	49
[Zn(MeIm)$_3$(EtIm)$_3$][Tf$_2$N]$_2$	35
[Zn(MeIm)$_2$(EtIm)$_4$][Tf$_2$N]$_2$	20
[Zn(MeIm)$_1$(EtIm)$_5$][Tf$_2$N]$_2$	29
[Zn(EtIm)$_6$][Tf$_2$N]$_2$	35
[Zn(BuIm)$_6$][Tf$_2$N]$_2$	<RT[a]

[a] Liquid at room temperature.

melting point of 20 °C, which is well below that of both the homoleptic [Zn(MeIm)$_6$][Tf$_2$N]$_2$ and [Zn(EtIm)$_6$][Tf$_2$N]$_2$ compounds.

It is also interesting to compare the melting behaviour with similar cobalt(II), nickel(II) and copper(II) complexes of the formula $[M(MeIm)_6][Tf_2N]_2$ (M = Ni, Co, Cu, Zn). Previously, we found that the cobalt(II) and nickel(II) analogues had high melting points (137 and 147 °C, respectively), whilst $[Cu(MeIm)_6][Tf_2N]_2$ had a much lower melting point (52 °C).[22] This low melting point was ascribed to the weakly bound ligands in the axial position of the Jahn–Teller distorted Cu(II) complex and the transformation on melting to the complex $[Cu(MeIm)_4][Tf_2N]_2$ and MeIm. The melting point of $[Zn(MeIm)_6][Tf_2N]_2$ (65 °C) is much closer to that of the copper(II) complex, which is quite surprising as the M–N bond distances and coordination environment are much closer to those in the cobalt(II) and nickel(II) analogues. However, it is a possibility that there is incongruent melting and there is a transformation of the Zn(II) complex into the coordination number of four to form the complex $[Zn(MeIm)_4][Tf_2N]_2$ and MeIm.

Thermogravimetric analysis (TGA) has been performed to check the thermal stability of the new Zn(II) compounds. The TGA traces (Fig. 5) show that $[Zn(MeIm)_6][Tf_2N]_2$, $[Zn(EtIm)_6][Tf_2N]_2$ and $[Zn(BuIm)_6][Tf_2N]_2$ are thermally stable below 100 °C. The compounds start to significantly lose mass at temperatures above 100 °C and a plateau is observed for the compounds $[Zn(MeIm)_6][Tf_2N]_2$ and $[Zn(EtIm)_6][Tf_2N]_2$ in the temperature range between 150 and 300 °C. The values of the corresponding remaining weight at these plateaus corresponds well to the theoretical mass losses of two N-alkylimidazole ligands from the coordination shell of the Zn(II) compounds, to form four-coordinate Zn(II) complexes. At temperatures above 250 °C the remaining N-alkylimidazole ligands are quickly lost. For $[Zn(BuIm)_6][Tf_2N]_2$ the BuIm ligands are initially lost more slowly than the MeIm and EtIm analogues and there is no plateau for the loss of two ligands; however, above 250 °C the mass loss is faster than for the MeIm and EtIm analogues. All the zinc(II)-containing liquid

metal salts had a thermal stability that was deemed enough for electrochemical studies at 90 °C and practice showed that this was indeed the case. The formation of a four-coordinate complex between 150 °C and 300 °C could suggest the occurrence of incongruent melting and the presence of free AlkIm ligands in the melt. However, it is difficult to extrapolate this behaviour at high temperatures to the temperatures between 25 °C and 100 °C and to draw the conclusion that the melt contains a four-coordinate complex. It is also a possibility that as the sample is heated and as the AlkIm ligands are lost, the six-coordinate complex is transformed into a four-coordinate one at those higher temperatures.

The viscosity of zinc(II)-containing liquid metal salts has been measured at 40 °C (where possible) and at 80 °C. The viscosity of $[Zn(MeIm)_6][Tf_2N]_2$ (T_m = 65 °C) was 13 mPa s at 80 °C. The viscosity of $[Zn(EtIm)_6][Tf_2N]_2$ (T_m = 35 °C) was found to be 63 mPa s (40 °C) and 16 mPa s (80 °C). The viscosity of $[Zn(BuIm)_6][Tf_2N]_2$ was found to be 162 mPa s (40 °C) and 28 mPa s (80 °C). These values are significantly lower in comparison with conventional room-temperature ionic liquids,[3,5] and previously reported zinc(II)-containing cationic complexes,[16] but similar to other N-alkylimidazole containing liquid metal salts.[18,19]

To further investigate the coordination number of the liquids, ^{15}N NMR spectra of the pure $[Zn(MeIm)_6][Tf_2N]_2$, $[Zn(EtIm)_6][Tf_2N]_2$ and $[Zn(BuIm)_6][Tf_2N]_2$ liquids were recorded (see ESI†). If the liquids contained a mixture of coordinated and uncoordinated AlkIm ligands, it may be possible to observe the resonances for the coordinated and uncoordinated nitrogen atoms, provided that the ligand exchange is slow enough on the NMR timescale. The spectra show that the nitrogen involved in coordination to the zinc(II) centre shifts approximately 50 ppm upfield in the coordinated complex compared to the free ligand. The other AlkIm ^{15}N resonances were shifted approximately 5 ppm downfield. The resonance of the nitrogen atom in the Tf_2N^- anion was at the same frequency for all complexes. There were no other resonances so it can be concluded that there are no free AlkIm ligands or that the exchange is too fast on the NMR timescale to detect the differences. Raman experiments, which can identify faster processes on the timescale, on solid and liquid samples of the liquid metal salts were inconclusive. There is also the possibility that both the six-coordinate complex and the four-coordinate complexes exist in the liquid state and that they are in equilibrium with each other. Due to the uncertain speciation of the liquid state, another possible way of describing the $[Zn(AlkIm)_6][Tf_2N]_2$ liquids would be $Zn(Tf_2N)_2·6AlkIm$.

Electrochemistry and electrodeposition

The electrochemical behaviour of the zinc(II)-containing liquid metal salts has been analysed by means of cyclic voltammetry and galvanostatic zinc electrodeposition on a platinum working electrode at 90 °C in an argon-filled glove box. This temperature was selected to ensure that all the tested liquid metal salts were in the liquid state and to promote mass transport by means of lowering viscosity. Fig. 6a shows the cyclic
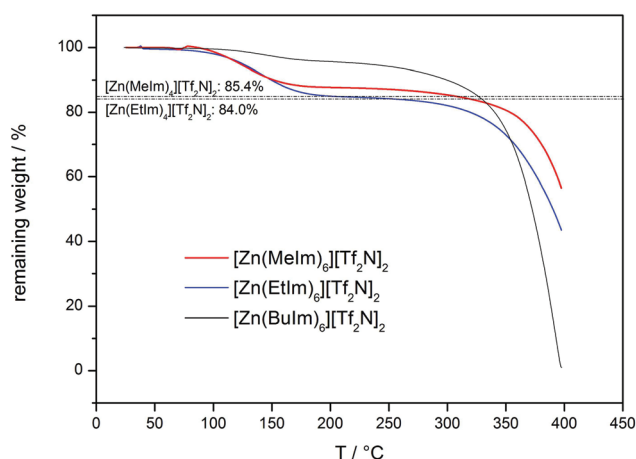
Fig. 5 TGA traces of $[Zn(MeIm)_6][Tf_2N]_2$, $[Zn(EtIm)_6][Tf_2N]_2$ and $[Zn(BuIm)_6][Tf_2N]_2$, the temperature was scanned from room temperature to 400 °C at 5 °C min^{-1}. The dashed lines correspond to the theoretical remaining mass percentages of $[Zn(MeIm)_4][Tf_2N]_2$ and $[Zn(EtIm)_4][Tf_2N]_2$ complexes after ligand losses.
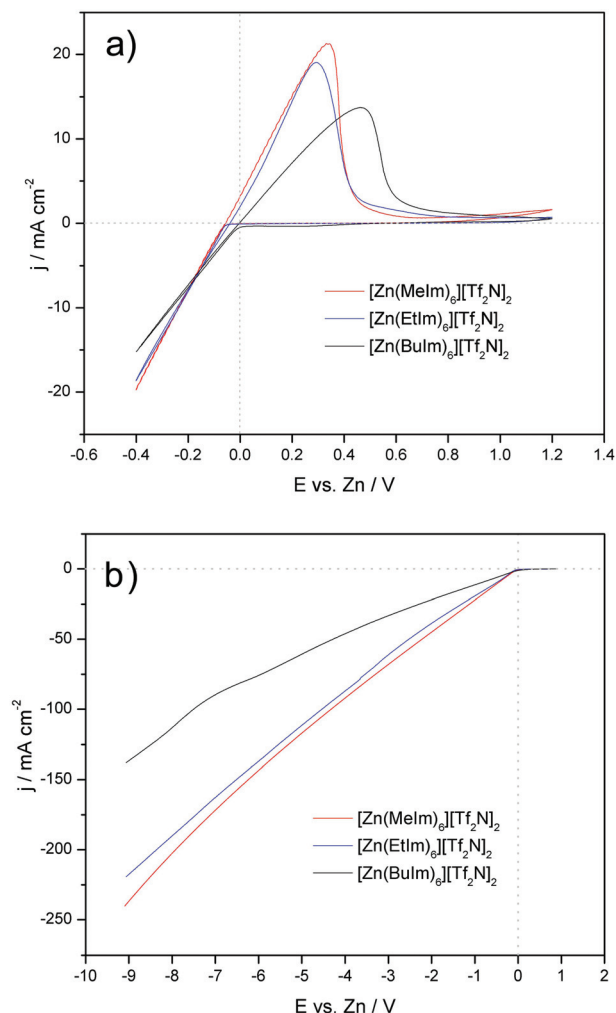
Fig. 6 (a) Cyclic voltammetry of homoleptic $[Zn(AlkIm)_6][Tf_2N]_2$ compounds on a platinum electrode (corrected for iR drop). (b) Linear sweep voltammetry of the corresponding homoleptic zinc(II) liquid metal salts on a platinum electrode (not corrected for iR drop). $T = 90$ °C, $v_{scan} = 20$ mV s^{-1}. Zinc was used as large-area counter-electrode and pseudo-reference electrode.

voltammograms of the homoleptic $[Zn(MeIm)_6][Tf_2N]_2$, $[Zn(EtIm)_6][Tf_2N]_2$, and $[Zn(BuIm)_6][Tf_2N]_2$ liquid metal salts at 90 °C at a scan rate of 20 mV s^{-1} between +1.2 V and −0.4 V. The presented CVs show the steady-state cycles of the electrolytes after 2–3 cycles. In the steady-state CVs, typical reversible metal electrodeposition–metal stripping behaviour during potential cycling was observed for all liquid metal salts. All zinc deposited during the cathodic scan was redissolved on the anodic backward scan: integration of the current densities in the cyclic voltammograms showed that the stripping efficiency Q_a/Q_c is close to 100%, where Q_a is the charge passed during the anodic stripping scan and Q_c is the charge passed during the cathodic deposition process. This implies that the reoxidation of the as-deposited zinc is a two-electron transfer process. At $E < 0.0$ V, very high current densities related to zinc electrodeposition were recorded and no peak currents, owing to diffusion limitations,[39] were observed for

the zinc(II) liquid metal salts. The high cathodic current densities depended on the N-alkylimidazole ligand composition of the zinc(II) liquid metal salts, in agreement with the Zn(II) concentration of $[Zn(MeIm)_6][Tf_2N]_2$, (1.49 M), $[Zn(EtIm)_6][Tf_2N]_2$ (1.35 M) and $[Zn(BuIm)_6][Tf_2N]_2$ (1.15 M). At −0.4 V, $[Zn(MeIm)_6][Tf_2N]_2$ and $[Zn(EtIm)_6][Tf_2N]_2$ presented higher current densities of −19.8 and −18.7 mA cm^{-2}, respectively, compared to −15.2 mA cm^{-2} for the $[Zn(BuIm)_6][Tf_2N]_2$. Even though the $[Zn(BuIm)_6][Tf_2N]_2$ compound has a lower current density, the onset of zinc electrodeposition in this liquid metal salt was observed at lower overpotentials compared to the analogues with shorter alkyl chains, $[Zn(MeIm)_6][Tf_2N]_2$ and $[Zn(EtIm)_6][Tf_2N]_2$. It can be speculated that this lower deposition onset potential is related to weaker binding of the BuIm ligands to the zinc(II) centre.[39] The cathodic current density at −0.4 V of $[Zn(MeIm)_3(EtIm)_3][Tf_2N]_2$ is −18.8 mA cm^{-2}, which is close to that of $[Zn(EtIm)_6][Tf_2N]_2$.

In order to evaluate the highest current densities that can be achieved during zinc electrodeposition from the synthesised zinc(II)-containing liquid metal salts, linear potential scans to higher cathodic overpotentials have been performed (Fig. 6b). As expected for electrolytes with high metal concentrations and low viscosity, the cathodic currents increased linearly with the applied potential and no drop-off of the cathodic currents was observed in the unstirred solutions. High current densities above −200 mA cm^{-2} were recorded for $[Zn(MeIm)_6]$-$[Tf_2N]_2$ and $[Zn(EtIm)_6][Tf_2N]_2$ at $E < -8.5$ V versus Zn. Similar high deposition current densities of more than −200 mA cm^{-2} could be obtained for the corresponding heteroleptic $[Zn-(MeIm)_3(EtIm)_3][Tf_2N]_2$ compound. For $[Zn(BuIm)_6][Tf_2N]_2$, a current density only slightly above −150 mA cm^{-2} was achieved. Based on these voltammetry experiments, it can be concluded that the zinc(II) complexes with the shorter alkyl chains are good candidates for high current density electrodeposition of zinc.

It was shown that the electrodeposition process from the new zinc(II) liquid metal salts are not limited by mass transport, even not at high cathodic overpotentials. Therefore, the electron transfer kinetics of the reversible zinc deposition–stripping reaction can be analysed using the Butler–Volmer equation:[39]

$$i = i_0 \left[\exp\left(\frac{\alpha nF}{RT}\eta\right) - \exp\left(-\frac{(1-\alpha)nF}{RT}\eta\right) \right], \quad (1)$$

where i_0 is the exchange current density (mA cm^{-2}), α is the charge transfer coefficient ($0 < \alpha < 1$), n is the number of transferred electrons ($n = 2$), η ($= E - E_{eq}$) is the overpotential (V), R is the ideal gas constant (8.314 J mol^{-1} K^{-1}), F is the Faraday constant (96 485 C mol^{-1}) and T is the temperature (K). The electron transfer kinetic parameters of the Zn(II)/Zn couple on platinum were determined by Tafel analysis:[39]

$$\log |i| = \log i_0 - \frac{\alpha nF}{2.3 RT}\eta, \quad \text{for the cathodic branch} \quad (2)$$

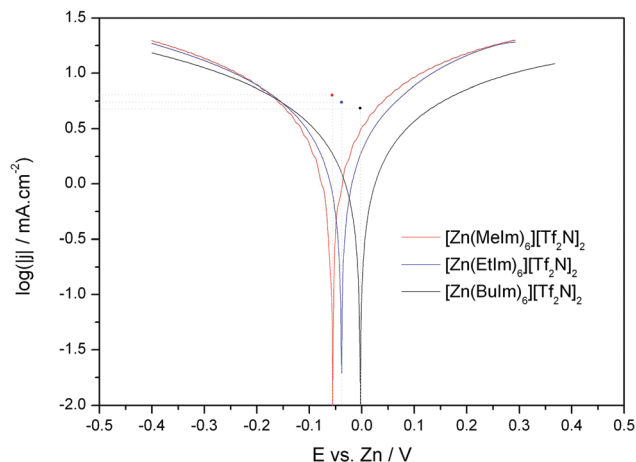$$\log |i| = \log i_0 + \frac{(1-\alpha)nF}{2.3 RT}\eta, \quad \text{for the anodic branch} \quad (3)$$

Fig. 7 Tafel plots of the homoleptic [Zn(AlkIm)$_6$][Tf$_2$N]$_2$, extracted from the backward scans of the cyclic voltammograms of Fig. 6.

Table 5 Kinetic parameters of the Zn(II)/Zn redox couple in the homoleptic [Zn(AlkIm)$_6$][Tf$_2$N]$_2$ at 90 °C

Compound	E_{eq}/mV	α	i_0/mA cm^{-2}
[Zn(MeIm)$_6$][Tf$_2$N]$_2$	−55 (±2)	0.51	6.4
[Zn(EtIm)$_6$][Tf$_2$N]$_2$	−38 (±2)	0.50	5.4
[Zn(BuIm)$_6$][Tf$_2$N]$_2$	−2 (±2)	0.49	4.9

According to eqn (2) and (3), the exchange current density i_0 can be determined from the intercept at the equilibrium potential E_{eq} (η = 0) and the charge transfer coefficient α is given by the slope of the anodic and cathodic branches at $|\eta| \geq 0.2$ V.

Fig. 7 shows the Tafel plot of the backward scan from the CVs of the homoleptic [Zn(AlkIm)$_6$][Tf$_2$N]$_2$ compounds on platinum in Fig. 6a. The kinetic parameters E_{eq}, α and i_0 of the Zn(II)/Zn couple in the three homoleptic zinc(II) compounds are compared in Table 5. The reversibility of the systems is observed by the symmetric anodic and cathodic branches of the Tafel plots and the charge transfer coefficient α close to 0.5.

From the Tafel plots it is observed that the equilibrium potentials E_{eq} shift to more negative potentials as the alkyl chain length of the N-alkylimidazole ligand decreases. This follows the same trend as the deposition onset potential shifts observed in Fig. 6 and suggests the stronger coordination to the zinc(II) centre of the N-alkylimidazole ligands with shorter alkyl chain length, even though small potential shifts of the pseudo-reference electrode cannot be fully excluded. As for the exchange current density, the highest values have been found for [Zn(MeIm)$_6$][Tf$_2$N]$_2$ followed by [Zn(EtIm)$_6$][Tf$_2$N]$_2$ and [Zn(BuIm)$_6$][Tf$_2$N]$_2$, in agreement with the current densities observed in cyclic voltammetry. The determined exchange current densities of the highly concentrated Zn(II)-LMS (ca. 1 M) are several orders of magnitude higher than values determined for imidazolium and pyrrolidinium room-temperature ionic liquids containing 0.1 M zinc(II) bis(trifluoromethylsulfo-

nyl)imide salt, for which low values between 2.3 and 9.9 μA cm^{-2} have been measured.[40] For comparison, in aqueous alkaline and acid zinc plating baths exchange current densities ranging from 20 to 100 mA cm^{-2} have been reported.[1] With such high exchange current density values, the electrodeposition is expected to be diffusion-controlled at high overpotentials and the use of organic additives and/or precise hydrodynamic control of the electrolytes are necessary to obtain dense, compact zinc coatings and to avoid the formation of zinc dendrites. In all zinc(II)-containing liquid metal salts, n is close to 2. These observations confirm the measured stripping efficiency of close to 100% during cyclic voltammetry and suggest that the Zn(II)/Zn redox couple follows a reversible, single-step, two-electron reaction in the zinc(II) liquid metal salts.

The synthesised liquid metal salts have been used for the electrodeposition of zinc metal films at high current density. Galvanostatic electrodepositions were performed on platinum electrodes at 90 °C in unstirred solutions. The deposits were analysed by SEM/EDX and XRD. The morphology was only slightly influenced by the N-alkylimidazole ligand composition of the liquid metal salts. In general, smooth, crystalline, crack-free and compact zinc deposits were obtained from the homo- and heteroleptic zinc(II) liquid metal salts at 90 °C. Fig. 8a shows a representative SEM top-view and Fig. 8b shows the corresponding cross-section micrographs of a zinc film electro-
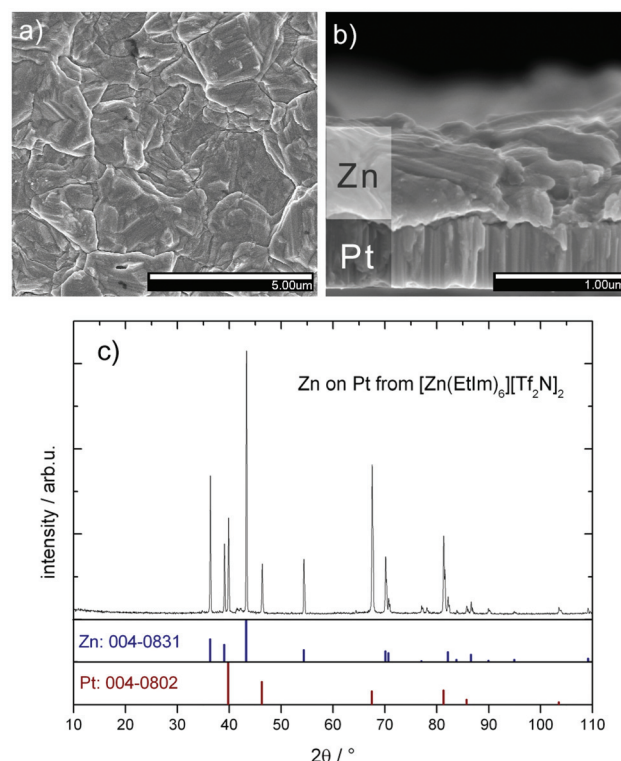

Fig. 8 SEM (a) top-view and (b) cross-section micrographs and (c) the corresponding XRD diffractogram of a zinc deposit on a platinum electrode from [Zn(EtIm)$_6$][Tf$_2$N]$_2$, j_{dep} = −100 mA cm^{-2}, 20 s, 90 °C. Reference patterns of zinc (JCPDS: 004-0831) and platinum (JCPDS: 004-0802) are included for comparison.

deposited from $[\text{Zn}(\text{EtIm})_6][\text{Tf}_2\text{N}]_2$ on platinum at a current density of -100 mA cm^{-2} for 20 s at 90 °C. The SEM top-view (Fig. 8a) clearly shows that highly crystalline and compact zinc deposits can be produced. EDX analysis showed that the deposit is solely composed of metallic zinc. Within the EDX detection limits (*ca.* 0.5 at%), no contaminations originating from the liquid metal salts could be detected in the deposits. Large zinc crystals with diameters of up to 5 μm are observed. The SEM cross-sectional image (Fig. 8b) confirms the crystallinity and the compactness of the zinc film on the Pt substrate. Covering and dense zinc films without voids were obtained. Assuming a plating efficiency of 100% and neglecting the double layer charging effects under these deposition conditions, a theoretical film thickness of 950 nm is expected.

X-ray diffraction performed on the same deposit from $[\text{Zn}(\text{EtIm})_6][\text{Tf}_2\text{N}]_2$ on platinum at a current density of -100 mA cm^{-2} for 20 s at 90 °C shows that the deposit is highly crystalline and the resulting diffractogram (Fig. 8c) contains peaks from only zinc and the platinum substrate (see reference patterns of zinc (JCPDS: 004-0831) and platinum (JCPDS: 004-0802)). Minor Bragg peaks corresponding to Pt$_x$Zn$_y$ alloys have been recorded at θ = 41.5, 42.2 and 78.2° showing that there is a formation of these alloys during the high-speed electrodeposition at 90 °C, in agreement with the platinum–zinc phase diagram.[41] Platinum–zinc alloying is also observed during the electrodeposition of zinc on platinum electrodes from sulphate electrolytes (pH 1.0–1.6). In these electrolytes, zinc bulk electrodeposition is proceeded by hydrogen evolution reaction, zinc underpotential deposition and platinum–zinc alloy formation.[42]

The average coherence length D of the zinc crystals can be estimated from the main Zn(101) Bragg peak, using the Scherrer formula:

$$D = \frac{k\lambda}{\beta \cos(\theta)}, \qquad (4)$$

where D is the average coherence length in nm, k = 0.9 is the shape factor, λ = 1.54056 Å is the wavelength of the incident radiation, β is the full width at half maximum FWHM in rad and θ is the Bragg angle in rad. The FWHM of the main Zn(101) reflection of the deposits formed in $[\text{Zn}(\text{EtIm})_6][\text{Tf}_2\text{N}]_2$ is 0.13° and gives an average coherence length D = 840 nm. As the crystals are not of spherical symmetry, the values have to be considered as approximations. Nevertheless, the determined crystal size is of the same order of magnitude as the film thickness observed in the SEM and the theoretical thickness of 950 nm. This suggests that the as-deposited zinc crystals extend from top to bottom in the dense film to completely cover the platinum surface, as is also seen in the SEM cross-section (Fig. 8b).

Conclusion

In summary, cationic zinc(ɪɪ) complexes with *N*-alkylimidazole ligands, in combination with the bis(trifluoromethylsulfonyl)imide (Tf_2N^-) anion, have been synthesised and characterised and found to be room temperature ionic liquids or having melting points slightly above room temperature. We have shown that the melting point can be tuned between 65 °C and below room temperature, as a function of the alkyl chain length in the homoleptic $[\text{Zn}(\text{AlkIm})_6][\text{Tf}_2\text{N}]_2$ complexes and as a function of the composition of the *N*-alkylimidazole ligands in the heteroleptic complexes $[\text{Zn}(\text{AlkIm})_{6-x}(\text{AlkIm}')_x][\text{Tf}_2\text{N}]_2$. Single crystal X-ray diffraction revealed that in addition to the homoleptic compounds, $[\text{Zn}(\text{MeIm})_6][\text{Tf}_2\text{N}]_2$ and $[\text{Zn}(\text{EtIm})_6]$-$[\text{Tf}_2\text{N}]_2$ crystals of heteroleptic compounds also crystallised. $[\text{Zn}(\text{MeIm})(\text{EtIm})_5][\text{Tf}_2\text{N}]_2$ and $[\text{Zn}(\text{MeIm})_2(\text{EtIm})_4][\text{Tf}_2\text{N}]_2$ were found to be isostructural to $[\text{Zn}(\text{EtIm})_6][\text{Tf}_2\text{N}]_2$, but $[\text{Zn}(\text{MeIm})_{4.5}(\text{EtIm})_{1.5}][\text{Tf}_2\text{N}]_2$ had a completely different structure from either of the homoleptic compounds. The cationic zinc(ɪɪ) complexes were shown to have low viscosities and to be electroactive and suitable for the high current density electrodeposition of zinc at temperatures above their melting points. Even at very high overpotentials, the deposition is not limited by mass transport in the melt. High exchange current densities were determined and allowed the deposition of dense and highly crystalline zinc deposits at high current densities in unstirred solutions.

Acknowledgements

References

1 *Modern Electroplating*, ed. E. Schlesinger and M. Paunovic, Wiley, 4th edn, 2000.

2 T. Welton, *Chem. Rev.*, 1999, **99**, 2071–2083.

3 N. V. Plechkova and K. R. Seddon, *Chem. Soc. Rev.*, 2008, **37**, 123–150.

4 M. Armand, F. Endres, D. R. MacFarlane, H. Ohno and B. Scrosati, *Nat. Mater.*, 2009, **8**, 621–629.

5 *Electrodeposition from Ionic Liquids*, ed. F. Endres, A. P. Abbott and D. R. MacFarlane, Wiley-VCH, Weinheim, 2008.

6 S. Z. El Abedin and F. Endres, *ChemPhysChem*, 2006, 7, 58–61.

7 W. Simka, D. Puszczyk and G. Nawrat, *Electrochim. Acta*, 2009, **54**, 5307–5319.

8 M. Steichen, M. Thomassey, S. Siebentritt and P. J. Dale, *Phys. Chem. Chem. Phys.*, 2011, **13**, 4292–4302.

9 G. T. Cheek, W. E. O'Grady, S. Z. El Abedin, E. M. Moustafa and F. Endres, *J. Electrochem. Soc.*, 2008, **155**, D91–D95.

10 S. Z. El Abedin, E. M. Moustafa, R. Hempelmann, H. Natter and F. Endres, *Electrochem. Commun.*, 2005, **7**, 1111–1116.

11 M. Steichen, R. Djemour, L. Guetay, J. Guillot, S. Siebentritt and P. J. Dale, *J. Phys. Chem. C*, 2013, **117**, 4383–4393.

12 P. Nockemann, B. Thijs, S. Pittois, J. Thoen, C. Glorieux, K. Van Hecke, L. Van Meervelt, B. Kirchner and K. Binnemans, *J. Phys. Chem. B*, 2006, **110**, 20978–20992.

13 A. E. Visser, R. P. Swatloski, W. M. Reichert, R. Mayton, S. Sheff, A. Wierzbicki, J. J. H. Davis and R. D. Rogers, *Chem. Commun.*, 2001, 135–136.

14 P. Nockemann, M. Pellens, K. Van Hecke, L. Van Meervelt, J. Wouters, B. Thijs, E. Vanecht, T. N. Parac-Vogt, H. Mehdi, S. Schaltin, J. Fransaer, S. Zahn, B. Kirchner and K. Binnemans, *Chem. – Eur. J.*, 2010, **16**, 1849–1858.

15 H. D. Pratt III, J. C. Leonard, L. A. M. Steele, C. L. Staiger and T. M. Anderson, *Inorg. Chim. Acta*, 2013, **396**, 78–83.

16 H. D. Pratt III, A. J. Rose, C. L. Staiger, D. Ingersoll and T. M. Anderson, *Dalton Trans.*, 2011, **40**, 11396–11401.

17 S. Schaltin, N. R. Brooks, K. Binnemans and J. Fransaer, *J. Electrochem. Soc.*, 2011, **158**, D21–D27.

18 S. Schaltin, N. R. Brooks, L. Stappers, K. Van Hecke, L. Van Meervelt, K. Binnemans and J. Fransaer, *Phys. Chem. Chem. Phys.*, 2012, **14**, 1706–1715.

19 D. Depuydt, N. R. Brooks, S. Schaltin, L. Van Meervelt, J. Fransaer and K. Binnemans, *ChemPlusChem*, 2013, **78**, 578–588.

20 N. R. Brooks, S. Schaltin, K. Van Hecke, L. Van Meervelt, J. Fransaer and K. Binnemans, *Dalton Trans.*, 2012, **41**, 6902–6905.

21 N. R. Brooks, S. Schaltin, K. Van Hecke, L. Van Meervelt, K. Binnemans and J. Fransaer, *Chem. – Eur. J.*, 2011, **17**, 5054–5059.

22 T. Vander Hoogerstraete, N. R. Brooks, B. Norberg, J. Wouters, K. Van Hecke, L. Van Meervelt and K. Binnemans, *CrystEngComm*, 2012, **14**, 4902–4911.

23 M. Kar, B. Winther-Jensen, M. Forsyth and D. R. MacFarlane, *Phys. Chem. Chem. Phys.*, 2013, **15**, 7191–7197.

24 T. J. Simons, A. A. J. Torriero, P. C. Howlett, D. R. MacFarlane and M. Forsyth, *Electrochem. Commun.*, 2013, **18**, 119–122.

25 S. I. Hsiu, J. F. Huang, I. W. Sun, C. H. Yuan and J. Shiea, *Electrochim. Acta*, 2002, **47**, 4367–4372.

26 T. Iwagishi, H. Yamamoto, K. Koyama, H. Shirai and H. Kobayashi, *Electrochemistry*, 2002, **70**, 671–674.

27 K. Koyama, T. Iwagishi, H. Yamamoto, H. Shirai and H. Kobayashi, *Electrochemistry*, 2002, **70**, 178–182.

28 A. P. Abbott, G. Capper, D. L. Davies, H. Munro, R. K. Rasheed and V. Tambyrajah, in *Ionic Liquids as Green Solvents: Progress and Prospects*, 2003, vol. 856, pp. 439–452.

29 Y. F. Lin and I. W. Sun, *Electrochim. Acta*, 1999, **44**, 2771–2777.

30 J. F. Dai, W. Wang, J. Liang, Q. W. Chu and Z. Z. Zhen, *Surf. Eng.*, 2013, **29**, 500–506.

31 Z. Liu, S. Z. El Abedin and F. Endres, *Electrochim. Acta*, 2013, **89**, 635–643.

32 Z. Liu, A. Prowald, S. Z. El Abedin and F. Endres, *J. Solid State Chem.*, 2013, **17**, 1185–1188.

33 J. A. Welleman, F. B. Hulsbergen, J. Verbiest and J. Reedijk, *J. Inorg. Nucl. Chem.*, 1978, **40**, 143–147.

34 J. F. Huang, H. M. Luo and S. Dai, *J. Electrochem. Soc.*, 2006, **153**, J9–J13.

35 *CrysAlisPRO*, Agilent Technologies, Yarnton, Oxfordshire, UK, 2011.

36 G. M. Sheldrick, *Acta Crystallogr., Sect. A: Fundam. Crystallogr.*, 2008, **64**, 112–122.

37 O. V. Dolomanov, L. J. Bourhis, R. J. Gildea, J. A. K. Howard and H. Puschmann, *J. Appl. Crystallogr.*, 2009, **42**, 339–341.

38 J. Sniekers, N. R. Brooks, S. Schaltin, L. Van Meervelt, J. Fransaer and K. Binnemans, *Dalton Trans.*, 2014, **43**, 1589–1598.

39 A. J. Bard and L. R. Faulkner, *Electrochemical methods: fundamentals and applications*, John Wiley & Sons, Inc., New York, 2001.

40 M. Xu, D. G. Ivey, Z. Xie and W. Qu, *Electrochim. Acta*, 2013, **89**, 756–762.

41 Z. Moser, in *Journal of Phase Equilibria*, Springer, 1991, vol. 12, pp. 439–443.

42 T. Boiadjieva, M. Monev, A. Tomandl, H. Kronberger and G. N. Fafilek, *J. Solid State Electrochem.*, 2009, **13**, 671–677.